

Synthesis of optical filters using microring resonators with ultra-large FSR

Salvador Vargas^{1,2,*} and Carmen Vazquez¹

¹Department of Electronic Technology, Universidad Carlos III de Madrid, Ave. Universidad No. 30, C.P: 28911, Leganés, Madrid, Spain

²Electrical Engineering Faculty, Universidad Tecnológica de Panamá, Ave. Universidad Tecnológica, El Dorado 0819-07289, Panamá, Panama

*sevargas@ing.uc3m.es

Abstract: We propose a novel synthesis method for designing flexible, tunable non-periodic filters. It is based on a building block which is presented by first time for these purposes, being the poles position tuned by means of a coupling coefficient and an amplifier gain. We present the device, the design equations and a design of a filter with flat response, 54 dB of crosstalk and less than 1.3 dB of ripple to explain and validate the method. These filters can be used as part of optical cross-connects for selecting channels avoiding very restrictive free spectral ranges. Also we check the correct operation of the device, against fabrication tolerances of coupling coefficients. Frequency dependence of the transfer function poles as a unique feature improving the crosstalk of the device spectral response is also analyzed.

©2010 Optical Society of America

OCIS codes: (230.3990) Micro-optical devices; (050.2770) Gratings; (350.2460) Filters, interference.

References and links

1. K. Jinguji, and T. Yasui, "Synthesis of One-Input M-Output Optical FIR Lattice Circuits," *J. Lightwave Technol.* **26**(7), 853–866 (2008).
2. A. Melloni, "Synthesis of a parallel-coupled ring-resonator filter," *Opt. Lett.* **26**(12), 917–919 (2001).
3. V. Van, "Circuit-Based Method for Synthesizing Serially Coupled Microring Filters," *J. Lightwave Technol.* **24**(7), 2912–2919 (2006).
4. N. Ngo, "Synthesis of Tunable Optical Waveguide Filters Using Digital Signal Processing Technique," *J. Lightwave Technol.* **24**(9), 3520–3531 (2006).
5. C. K. Madsen, "General IIR Optical Filter Design for WDM Applications Using All-Pass Filters," *J. Lightwave Technol.* **18**(6), 860–868 (2000).
6. K. Jinguji, "Synthesis of Coherent Two-Port Optical Delay-Line Circuit with Ring Waveguides," *J. Lightwave Technol.* **14**(8), 1882–1898 (1996).
7. K. Sasayama, M. Okuno, and K. Habara, "Coherent Optical Transversal Filter using silica-based single-mode waveguides," *Electron. Lett.* **25**(22), 1508–1509 (1989).
8. V. Van, "Dual-Mode Microring Reflection Filters," *J. Lightwave Technol.* **25**(10), 3142–3150 (2007).
9. S. Vargas, and C. Vazquez, "Synthesis of Optical Filters Using Sagnac Interferometer in Ring Resonator," *IEEE Photon. Technol. Lett.* **19**(23), 1877–1879 (2007).
10. S. Xiao, M. H. Khan, H. Shen, and M. Qi, "Silicon-on-Insulator Microring Add-Drop Filters With Free Spectral Ranges Over 30 nm," *J. Lightwave Technol.* **26**(2), 228–236 (2008).
11. Q. Xu, D. Fattal, and R. G. Beausoleil, "Silicon microring resonators with 1.5-microm radius," *Opt. Express* **16**(6), 4309–4315 (2008).
12. J. García, A. Martínez, and J. Martí, "Proposal of an OADM configuration with ultra-large FSR combining ring resonators and photonic bandgap structures," *Opt. Commun.* **282**(9), 1771–1774 (2009).
13. C. Vázquez, and O. Schwelb, "Tunable, narrow-band, grating-assisted microring reflectors," *Opt. Commun.* **281**(19), 4910–4916 (2008).
14. D. G. Rabus, M. Hamacher, U. Troppenz, and H. Heidrich, "High Q-Channel Dropping Filters Using Ring Resonators with Integrated SOAs," *IEEE Photon. Technol. Lett.* **14**(10), 1442–1444 (2002).
15. J. S. Yang, J. W. Roh, S. H. Ok, D. H. Woo, Y. T. Byun, W. Y. Lee, T. Mizumoto, and S. Lee, "An integrated optical waveguide isolator based on multimode interference by wafer direct bonding," *IEEE Trans. Magn.* **41**(10), 3520–3522 (2005).
16. W. Van Parys, D. Van Thourhout, R. Baets, B. Dagens, J. Decobert, O. Le Gouezigou, D. Make, and L. Lagae, "Amplifying Waveguide Optical Isolator with an Integrated electromagnet," *IEEE Photon. Technol. Lett.* **19**(24), 1949–1951 (2007).

17. C. Vazquez, S. Vargas, and J. M. S. Pena, "Sagnac Loop in Ring Resonators for Tunable Optical Filters," *J. Lightwave Technol.* **23**(8), 2555–2567 (2005).
 18. H. Stoll, "Optimally Coupled, GaAs-Distributed Bragg Reflection Lasers," *IEEE Trans. Circ. Syst.* **26**(12), 1065–1072 (1979).
 19. Q. Xu, I. Cremmos, O. Schwelb, and N. Uzunogly, *Photonic Microresonator Research and Applications* (Springer New York 2010), Chap. 9.
 20. Y. A. Vlasov, and S. J. McNab, "Losses in single-mode silicon-on-insulator strip waveguides and bends," *Opt. Express* **12**(8), 1622–1631 (2004).
 21. M. Gnan, S. Thoms, D. S. Macintyre, R. M. De La Rue, and M. Sorel, "Fabrication of low-loss photonic wires in silicon-on-insulator using hydrogen silsesquioxane electron-beam resis," *Electron. Lett.* **44**(2), 115–116 (2008).
 22. J. Proakis and D. Manolakis, *Digital Signal Processing*, (Prentice Hall 2006).
-

1. Introduction

The synthesis of optical delay lines filters, from building block like Mach Zehnder interferometers (MZI) [1], single ring resonators (RR) [2,3], and compound ring resonators (CRR) [4–6] have been widely used to generate filters with arbitrary transfer functions. These building blocks have been combined in transversal [7], lattice [1], and cascade [6] structures, resulting in filters with infinite and finite impulse response.

Synthesis methods that use these building blocks, RR [8] and CCR [9], with counter-propagating modes, are also reported.

But with all of these methods, optical filters with periodic transfer functions are designed and its frequency period is named Free Spectral Range (FSR). This can be a restriction in applications where the bandwidth of all the channels to be transmitted is greater than the FSR. Wavelength division multiplexing (WDM) communication systems, with a potential bandwidth to cover from 1260 nm to 1675 nm, will need time delays in the order of 20 fs, for overcoming this restriction. These time delays require total lengths in the order of 2 μm , which are not practical in the case of curved waveguides as happens in RR or CRR. First, because of high loss [10] at radius of curvature of less than 0.3 μm , and second there are problems associated with the stabilization [11], a length variation of one over one thousand represents, a FSR change in the order of tens of gigahertz which is unacceptable. Most promising devices fabricated in silicon on insulator (SOI) technology have a 1.5 μm radius [11], and in other novel configurations including photonics bandgaps, FSR of 140 nm are achieved from 45 μm ring length [12].

An alternative to overcome this limitation is combining these delay line filters with devices including non periodic transfer functions in the building block.

In this paper, it is proposed a synthesis method for designing infinite impulse response filters with arbitrary transfer functions, and ideal infinite FSR. A microring resonator with a Michelson interferometer (MI), inside the ring, made of diffraction gratings (DG) is used. This device integrates a delay line filter, with a non-periodic transfer function, allowing the fabrication of devices with greater time delays and better stability. The integration of these two types of filters in a single building block, improves the spectral characteristics in comparison with cascading a periodic and non-periodic transfer functions devices. This novel transfer function has frequency dependent complex conjugated poles, generating better crosstalk.

This is the first time that this device is used for these applications, different to the one previously reported as a reflective laser mirror [13], constituting a basic building block in a novel synthesis method for designing optical filters. Apart from breaking the spectral periodicity, this topology presents a second order transfer function, only with one RR, and poles position is tunable by changing coupling coefficient and gain. The proposed synthesis method, based on simple closed equations, allows developing filters with any type of spectral response.

2. Device

The device to be used as a building block to synthesize non-periodic optical filters is presented in Fig. 1, and the list of symbols used is described on Table 1. This is a Michelson Interferometer (MI) and an optical amplifier [14], within a ring resonator (MIARR).

Table 1. List of Symbols at Fig. 1

Symbol	Significance
G	- bidirectional amplifier power gain
K_M, K_i, K_o	- power coupling coefficient of MI, input and output couplers respectively
$\gamma_M, \gamma_i, \gamma_o$	- excess loss coefficient of MI, input and output couplers respectively
L_x, L_M	- length position of output coupler and MI respectively
L_b	- Michelson interferometer arms length

The MI acts as a frequency selective reflector, allowing clockwise and counterclockwise propagation in the ring. This is made of a directional coupler for splitting the light and identical DG as frequency selective mirrors. These gratings are key components of the MIARR because they break the transfer function periodicity, for achieving ultra-large FSR. The arms of MI have the same length L_b , and the power coupling coefficient K_M is different to 0.5, to assure the MI reflects some light. There is an optical isolator in the input port to avoid reflections [15]. This can be replaced by an amplifying optical isolator, providing design flexibility and loss compensation [16].

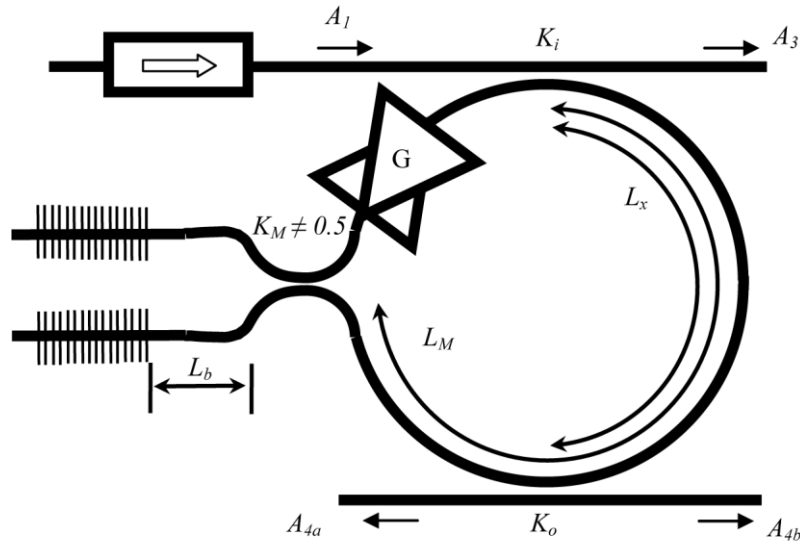


Fig. 1. Schematic of a MIARR.

Identical DG, to avoid dealing with two different reflection transfer functions is considered. Under this assumption the reflection and transmission transfer functions of the MI are given by:

$$FR = (1 - \gamma_M)(1 - 2K_M) r(\Omega) \quad (1)$$

$$FT = j2(1 - \gamma_M)(K_M(1 - K_M))^{1/2} r(\Omega) \quad (2)$$

where $r(\Omega)$, is the gratings reflectivity.

The output transfer function of the MIARR can be found using the transfer matrix formalism in the z domain, as explained in [17]. But first, the unitary delay τ has to be determined. This unitary delay is the total transit time in the RR. Which is given by $\tau = \tau_r + \tau_G$, where τ_r is the time delay due to waveguides length, including RR, couplers, amplifier and MI arms, and τ_G is the gratings group delay. This group delay is the negative derivative of the

diffraction gratings reflectivity phase $\phi_G(\Omega)$ with respect to Ω . This phase, under certain conditions, see [18], can be approximated by:

$$\phi_G(\Omega) = -\frac{\pi}{2} \left[\frac{n_{bef}}{\left(\alpha_b + \sqrt{k_b^2 + \alpha_b^2}\right)} \right] \left(\frac{\Omega - \Omega_G}{c} \right) \quad (3)$$

where k_b is the corrugation coupling coefficient, α_b the distributed loss coefficient, and n_{bef} the effective refractive index of gratings, c the vacuum light velocity, and Ω_G the center frequency (rad/seg) of diffraction gratings spectral response.

The grating group delay is given by:

$$\tau_G = \left[\frac{n_{bef}}{\left(\alpha_b + \sqrt{k_b^2 + \alpha_b^2}\right)} \right] \left(\frac{1}{c} \right) \quad (4)$$

This grating group delay, can be considered constant and can be included in the unitary delay τ . The gratings transfer function in the z domain, can be considered as that of a device that introduces a fraction of the unitary time delay of τ_G/τ . Diffraction gratings transfer function is given by:

$$DG(z) = -j |r(\Omega)| e^{-j\Delta\Omega\tau_G} = -j |r(\Omega)| z^{-\frac{\tau_G}{\tau}} \quad (5)$$

where we have taken $z = e^{j\Delta\Omega\tau}$, $\Delta\Omega = 2\pi(f - f_G)$, being f_G the center frequency of gratings transfer function.

Choosing the center frequency of diffraction grating Ω_G , equal to the resonance frequency of one of the longitudinal modes of the ring (with unitary delay τ), it makes that z in the rest of the transfer functions of the ring ($z = e^{j\Omega\tau}$) is equal to z in the diffraction grating transfer function [see Eq. (5)].

It can be calculated from [17] that the transfer functions of the MIARR at ports A_3 , A_{4a} , and A_{4b} are given by:

$$\frac{A_3}{A_1} = \frac{(1-\gamma_i)^{1/2} (1-Z_{c1}z^{-1}) (1-Z_{c2}z^{-1})}{(1-Z_p z^{-1}) (1-Z_p^* z^{-1})} \quad (6)$$

where $Z_{c1}(z)$ and $Z_{c2}(z)$ are given by:

$$Z_{c1}(z) = \frac{\left((1-\gamma_i)(1-\gamma_o)(1-K_o)G \right)^{1/2} (1-\gamma_M) |r(\Omega)| e^{-\alpha L_r}}{(1-K_i)^{1/2}} \times \left[(2-K_i)(K_M - K_M^2)^{1/2} + j \left((1-K_i)(1-2K_M)^2 - K_i^2 (K_M - K_M^2) \right)^{1/2} \right] \quad (7)$$

$$Z_{c2}(z) = \frac{\left((1-\gamma_i)(1-\gamma_o)(1-K_o)G \right)^{1/2} (1-\gamma_M) |r(\Omega)| e^{-\alpha L_r}}{(1-K_i)^{1/2}} \times \left[(2-K_i)(K_M - K_M^2)^{1/2} - j \left((1-K_i)(1-2K_M)^2 - K_i^2 (K_M - K_M^2) \right)^{1/2} \right] \quad (8)$$

where, α is attenuation coefficient and L_r is the waveguide lengths respectively.

$$\frac{A_{4a}}{A_1} = \frac{-((1-\gamma_i)(1-\gamma_o)K_i K_o)^{1/2} e^{-\alpha L_x}}{(1-Z_p z^{-1})(1-Z_p^* z^{-1})} \left[1 - 2(1-\gamma_M)((1-\gamma_i)(1-\gamma_o))^{1/2} \times \right. \\ \left. \times ((1-K_i)(1-K_o)(K_M - K_M^2)G)^{1/2} |r(\Omega)| e^{-\alpha L_r} z^{-1} \right] z^{-\frac{\tau_x}{\tau}} \quad (9)$$

$$\frac{A_{4b}}{A_1} = \frac{-(1-\gamma_o)(1-\gamma_M)(1-\gamma_i)^{1/2}}{(1-Z_p z^{-1})} \times \\ \times \frac{(K_i K_o (1-K_o))^{1/2} (1-2K_M) |r(\Omega)| e^{-\alpha(2L_M-L_x)} z^{-\frac{2\tau_M-\tau_x}{\tau}}}{(1-Z_p^* z^{-1})} \quad (10)$$

where, τ_M and τ_x , are the time delays due to the lengths L_M and L_x respectively.

From Eqs. (6), (9), and (10), it can be seen that the three output transfer functions have the same denominator, with two complex conjugated poles (Z_p and Z_p^*) which will be described later.

2.1 Output A_3

The transfer function at output A_3 , see Eq. (6), has two zeros. They are complex conjugated if the next relation is fulfilled:

$$K_i < \frac{-1 + \sqrt{1 + 4\Psi}}{2\Psi} ; \quad \Psi = \frac{(K_M - K_M^2)}{(1 - 2K_M)^2} \quad (11)$$

Otherwise, the zeros are real and different. The position of these zeros in the Z plane, near unitary circumference makes a sharper notch filter spectral response. Even the transfer function could have theoretically infinite crosstalk when placing them at the unitary circumference.

The module of complex conjugated zeros is given by:

$$|Z_c| = ((1-\gamma_i)(1-\gamma_o)(1-K_o)G)^{1/2} (1-\gamma_M) |r(\Omega)| e^{-\alpha L_r} \quad (12)$$

And from Eq. (12), theoretical limit, for infinite crosstalk when placing the zeros at the unitary circumference, can be achieved with a gain G given by:

$$G^{1/2} = \frac{1}{((1-\gamma_i)(1-\gamma_o)(1-K_o))^{1/2} (1-\gamma_M) |r(\Omega)| e^{-\alpha L_r}} \quad (13)$$

The frequency dependence of the zero module through $|r(\Omega)|$, see Eq. (12), can be interpreted in the spectral response. It means that it is possible to have a different radial position of the zero for each FSR of the ring, by changing the module value and therefore the crosstalk (depending on the $|r(\Omega)|$ value) in each period.

Otherwise, the angular position of the complex conjugated zeros is given by:

$$\varphi_z = \pm \tan^{-1} \left[\frac{((1-K_i)(1-2K_M)^2 - K_i^2 (K_M - K_M^2))^{1/2}}{(2-K_i)(K_M - K_M^2)^{1/2}} \right] \quad (14)$$

and it places the notches of the filter in frequencies given by:

$$f = f_G + \left(k \pm \frac{\varphi_z}{2\pi} \right) FSR; \quad k \in Z \quad (15)$$

For finding the zeros module in each FSR, we have to use the frequencies given in Eq. (15), to evaluate the $|r(\Omega)|$ in the Eq. (12).

From Eqs. (14) and (15), we see that using K_i and K_M the notches of the spectral response, can be placed from $-FSR/4$ to $+FSR/4$, from the resonance frequencies of the longitudinal modes of the ring, which are $f_G + k \times FSR$, for integer k .

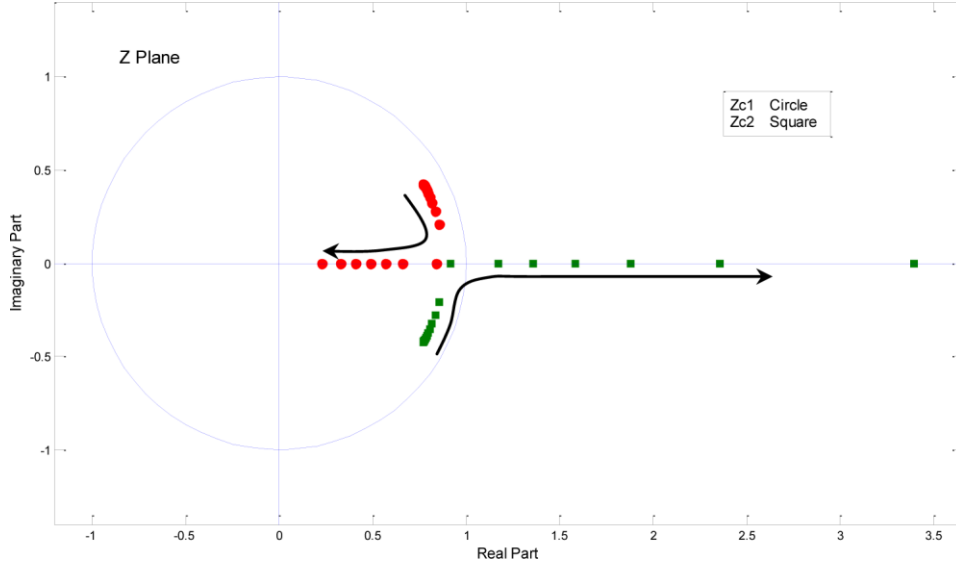


Fig. 2. Movement of zeros of the A_3/A_1 output transfer function, for increasing K_i from 0.05 to 0.95. $\alpha = 2\text{dB/cm}$, $\gamma_M = \gamma_i = \gamma_o = 0.05$, $K_M = 0.26$, $K_o = 0.05$, $G = 1$ and $|r(\Omega)| = 1$.

On the other hand, if the zeros are not complex conjugated, the zero modules are different, one is greater and the other is less than the value given in Eq. (12). They reach the infinite and zero values, in the limit when K_i tends to one. The phases of real zeros are zero, having the notch at the resonance frequencies of the longitudinal modes of the ring. In this case we use Eq. (15), with $\varphi_z = 0$ to evaluate $|r(\Omega)|$ in Eqs. (12).

In Fig. 2, it is shown the zero movement in Z plane, for increasing values of K_i from 0.05 to 0.95. The module of the zeros does not change, different to the phases, when they are complex conjugated. They have different values when they are real. In this simulation the $|r(\Omega)|$ took a value of one, being these the zeros position for the FSRs inside the central lobe of the ideal DG. For FSRs outside the central lobe of the DG, the module of the zeros is less due to $|r(\Omega)|$ values, ideally being equal to zero.

2.2 Output A_{4a}

The transfer function at output A_{4a} , is shown in Eq. (9). This output always has only one real positive zero that can be moved through the positive real axis of the Z plane, by increasing G . The value of G that places this zero in the unitary circumference is given by:

$$G^{1/2} = \frac{1}{2(1-\gamma_M) \left((1-\gamma_i)(1-\gamma_o)(1-K_i)(1-K_o)(K_M - K_M^2) \right)^{1/2} |r(\Omega)| e^{-\alpha L r}} \quad (16)$$

With this G value, we have a spectral response of a notch filter with theoretically infinite crosstalk, located at the resonance frequencies of the longitudinal modes of the ring. This

transfer function also has the term $z^{-cx/\tau}$, that arises to take into account the delay between the input and output pulses, because of the transit time in L_x .

2.3 Output A_{4b}

The transfer function at output A_{4b} , see Eq. (10), has complex conjugated poles, and a zero at the origin of the Z plane. This zero is fixed, and only introduces a constant delay in the transfer function. Because of these characteristics, against to the outputs A_{4a} and A_3 ; A_{4b} output transfer function can be used as an all pole function, for synthesizing filters with real coefficients.

The module and phase of the complex conjugated poles for the three outputs, see Eqs. (6), (9 - 10) are given by:

$$|Z_p| = (1 - \gamma_M) [(1 - \gamma_i)(1 - \gamma_o)(1 - K_i)(1 - K_o)G]^{1/2} |r(\Omega)| e^{-\alpha L r} \quad (17)$$

$$\varphi_p = \pm \tan^{-1} \left[\frac{(1 - 2K_M)}{2\sqrt{K_M(1 - K_M)}} \right] \quad (18)$$

The poles module $|Z_p|$ are frequency dependent, and different of zero only in the central lobe of the gratings spectral response, due to term $|r(\Omega)|$ in Eq. (17). This spectral response of the diffraction grating must be as close as possible to an ideal passband filter, with a maximum reflectivity of one. The frequency dependence of the poles module can be interpreted in the same form as the zeros in the previous transfer functions. There is a different radial position of the poles, for each FSR. Increasing or decreasing the peaks of the spectral response for each FSR. Depending on how far the poles are from the unitary circumference for these FSR. The Eq. (19) gives the gain value that locates the $|Z_p|$ in the unitary circumference, which gives theoretically infinite crosstalk.

$$G = \frac{1}{(1 - \gamma_M) [(1 - \gamma_i)(1 - \gamma_o)(1 - K_i)(1 - K_o)]^{1/2} |r(\Omega)| e^{-\alpha L r}} \quad (19)$$

The poles frequency dependence is basic for improving crosstalk as it is described in Section 5.

From Eq. (18), it can be seen that φ_p takes values between $-\pi/2$ to $\pi/2$, meaning that only in this margin it is possible to synthesize filters with complex conjugated poles. This could seem a drawback, but by increasing the FSR of the filter it can be increased the bandwidth of the synthesized filter, while maintaining the desired shape. The peaks position in frequency are given by Eq. (15), changing φ_z by φ_p . And we must use these frequencies to evaluate $|r(\Omega)|$ in Eq. (17), to find the poles module for each FSR.

The filter can be tuned, adjusting the center frequency of gratings (f_G) and the total delay time of the ring (τ), by means of the electro-optic effect or thermo-optic effect, heating or injecting current in the gratings and in the ring length [19]. The only requirement we should care about is making f_G to be located in one of the longitudinal resonant modes of the ring by any of the physical effects previously mentioned.

If this is not fulfilled, the poles will not be complex conjugated, appearing the complex term $e^{2\pi f_\Delta \tau}$ multiplying each pole (where f_Δ is the difference between f_G and the frequency of the nearest resonant mode of the ring). This term changes the poles position in the Z plane, rotating them $2\pi f_\Delta \tau$ radians, and increasing f_Δ Hz the peaks position in the spectral response, from its ideal position. The module of the poles can also be affected if there is a change in $|r(\Omega)|$. Finally, if the spectral response of the DG reflectivity is like an ideal bandpass filter; the spectral response will only be displaced in frequency.

3. Synthesis Equations

The synthesis procedure is similar to the one explained in [9], where cascaded second order all pole devices are used to synthesize the pairs of complex conjugated poles, an amplified ring resonator (ARR), and a lattice filter. In Fig. 3, we see the block diagram of the cascades stages. Here we use the MIARR as a second order device, taken the output A_{4b} , an ARR is used as in [9], with the same synthesis equations to synthesize the real pole, and a lattice filter, explained in Ref. [1]. for synthesizing the zeros. Also in Fig. 3, there is an amplifier stage (A) used for compensating the insertion loss due to the MIARR, ARR stages, and by the spectral response normalization step, in the algorithm of synthesizing the zeros by the lattice filter stage.

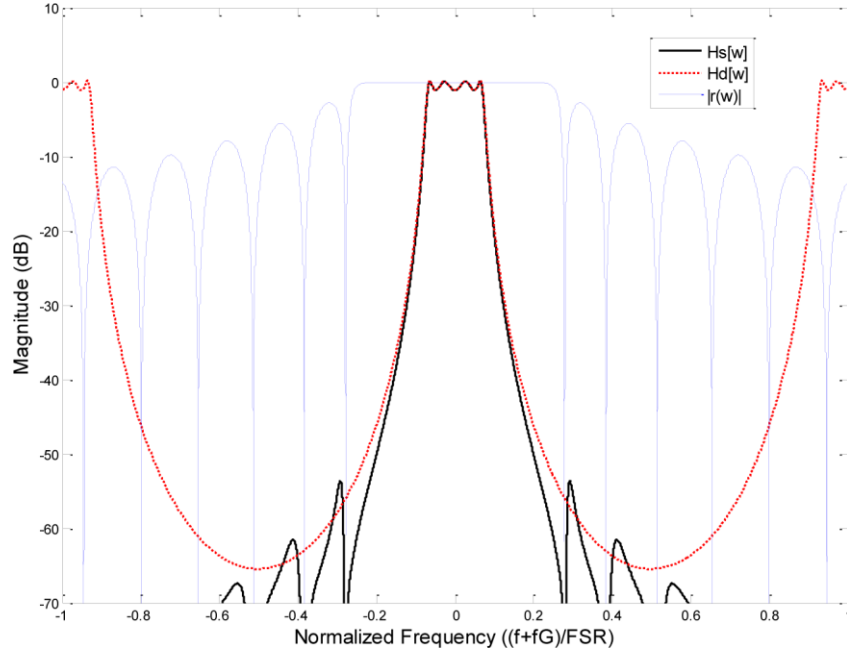


Fig. 3. Block diagram of cascaded stages.

In this paper, in comparison with the design method reported in [9], a different second order device is used, the MIARR, having a different set of equations. This device produces a non-periodic transfer function, and the poles position in the Z plane can be located, radial and angular, by means of, a gain and a coupling coefficient.

From Eqs. (10), (17), and (18) it can be seen that G , only appears in the poles module, making this parameter, ideal to be used for tuning the radial position of the poles. This selection is reinforced by the fact that the gratings must have a fix spectral response, and that K_i and K_o contribute to the loss introduced by the filter, see numerator of Eq. (10). These parameters are not suitable for tuning this radial location.

For selecting K_i and K_o values, filter loss are minimized once G is fixed. The following coupling coefficients are obtained:

$$K_i = \frac{1 - \chi}{1 + \chi} \quad (20)$$

$$K_o = \frac{1 - \chi}{2} \quad (21)$$

$$\text{with } \chi = \frac{|Z_p|^2}{(1-\gamma_M)^2(1-\gamma_i)(1-\gamma_o)G|r(\Omega_G + \varphi_p \cdot FSR)|^2 e^{-2\alpha Lr}} \quad (22)$$

The value of G is chosen arbitrary; but taking into account that it must be greater than a minimum value (G_{min}), to have positive K_i and K_o values. This minimum value is given by:

$$G_{min} > \frac{|Z_p|^2}{(1-\gamma_M)^2(1-\gamma_i)(1-\gamma_o)|r(\Omega_G + \varphi_p \cdot FSR)|^2 e^{-2\alpha Lr}} \quad (23)$$

Also we have to take into account that, as G increases χ decreases, which decreases the filter loss, see Eq. (20) and (21) and numerator of Eq. (10). Anyway, this loss can be compensated with the external gain stage A .

To locate the poles phases, K_M is used to change φ_p , see Eq. (18), to the value needed to synthesize the desired poles. The value of K_M , for a given pole phase, is given by:

$$K_M = \frac{1}{2} \pm \frac{1}{2} \sqrt{\frac{\tan^2(\varphi_p)}{1 + \tan^2(\varphi_p)}} \quad (24)$$

In Eq. (24), the positive or the negative sign, can be selected indistinctly, the change in the selection only sums π rads in the phase response, see Eq. (10).

4. Example and Discussion

For a better comprehension of the ultra-large FSR filter synthesis method, we present a detailed filter synthesis example. The desired transfer function ($Hd[z]$) to be synthesized is given by:

$$Hd[z] = \frac{0.0067z^{-2}}{1 - 3.4326z^{-1} + 4.5967z^{-2} - 2.8336z^{-3} + 0.6771z^{-4}} \quad (25)$$

This is a fourth order transfer function with two pairs of complex conjugated poles, as shown in Table 2, which means two stages of the MIARR are needed. The excess loss coefficient γ_i , γ_o and γ_M for the three couplers, are equal to 0.025 (0.1 dB/coupler) and the waveguide losses are 2 dB/cm [20,21], to simulate a SOI technology device at 1550 nm. To assure a unitary delay in the numerator of Eq. (5), in each one of the stages, we choose $\tau_M = 0.75\tau$ and $\tau_x = 0.5\tau$. The waveguide effective refractive index n_{ef} is 3.5, the parameters n_{bef} , α_p and k_b , of all the diffraction gratings used in the MIARR stages, are 3.6, 0 m⁻¹ and 480 m⁻¹, respectively. And the ratio FSR to full width at half maximum (FWHM) of gratings is chosen equal to 0.28.

The design procedure begins calculating the G_{min} for each stage; see Eq. (23), in this case 1.0817 and 0.9215 respectively. After an arbitrary value of G greater than G_{min} in the two stages is chosen; in this case G is selected to be equal to 2.1. Knowing the complex conjugated poles, modules and phases, and using Eqs. (20)–(24) the values of K_i , K_o , and K_M , for each stage are calculated. The loss introduced by the two stages filter, are then calculated, being 0.0052 for $G = 2.1$, here we can iteratively increase G , repeating the processes until the losses are 0.0067, the same value of the numerator of Eq. (25), being not necessary the gain stage A to compensate the losses. The final values are summarized in Table 2.

Table 2. MIARR Parameters Values per Stage; A = 1

Stage	$ Z_p $	ϕ_p	G_{min}	G	K_M	K_i	K_o
1	0.9442	± 0.4299	1.09	3	0.2916	0.47	0.3197
2	0.8715	± 0.1760	0.92	3	0.4125	0.53	0.3464

Another approximation is to use the minimum possible gain in the rings, see Eq. (23), and to compensate the losses by means of the external stage A. In this new approach, the found values are summarized in Table 3. Remember $G > G_{min}$, not equal.

Table 3. MIARR Parameters Values per Stage; $G = 1$

Stage	$ Z_p $	ϕ	G_{min}	G	K_M	K_i	K_o
1	0.9442	± 0.4299	1.09	1.3	0.2916	0.0917	0.0840
2	0.8715	± 0.1760	0.92	1	0.4125	0.0409	0.0393

In this case the loss is 199.5×10^{-6} , then a gain A of 33 should be used, a little more than 30 dB. These two solutions are extreme, but tailored intermediate solutions can be found, showing the flexibility of the design method.

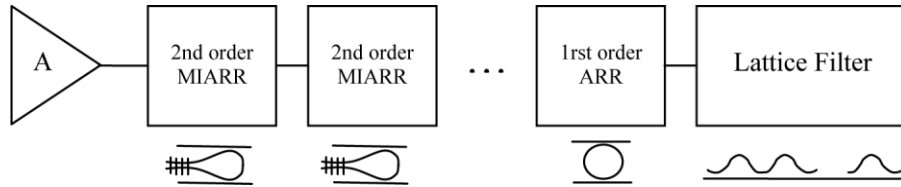


Fig. 4. Spectral response of synthesized $H_s[w]$, desired $H_d[w]$ and gratings transfer functions $r(w)$.

The spectral response of synthesized transfer function ($H_s[z]$) of the two stages MIARR filter, is shown in Fig. 4. A non-periodic transfer function is obtained, synthesized inside the diffraction grating bandwidth, also shown in this figure, with the shape of the desired transfer function $H_d[z]$ given in Eq. (25), which is also shown in this figure.

The synthesized filter transfer function shows excellent agreement with the ideal transfer function, with a less than 1.3 dB ripple, and a maximum crosstalk of 54 dB. This diminishing of the crosstalk from 65 dB of the desired transfer function, to the 54 dB of the synthesized transfer function, is due to the lateral lobes of the gratings.

These can be diminished using apodized gratings, increasing the crosstalk [12]. In Fig. 4 are shown lateral lobes of the gratings incorporated in the spectral response of $H_s[z]$.

As shown in Fig. 4, the synthesized filter has a non periodic spectral response, being his FSR very large or even infinite.

5. Variation of coupling coefficients and poles frequency dependence

In this section, it is analyzed, how the variation of the coupling coefficients of the couplers, due to fabrication tolerances, slightly affects the performance of the filter. It is also analyzed the poles frequency dependence in the filter, and its consequences. In all cases, the first filter designed in the previous section is used.

5.1 Variation of coupling coefficients

The coupling coefficients, for each stage of the MIARR used to synthesize the desired filter can vary from their theoretical values. This fact can alter the performance of the synthesized filter, changing the spectral response.

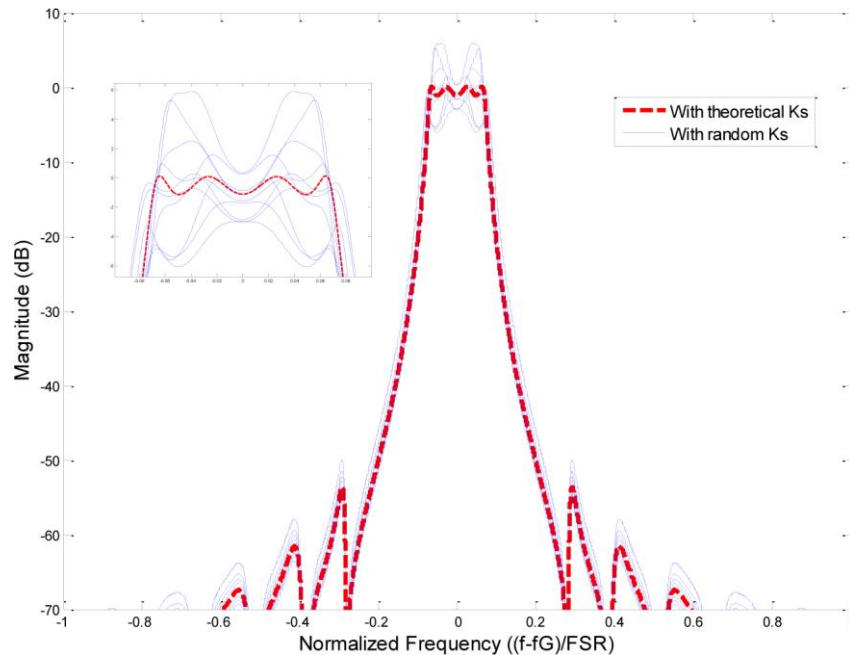


Fig. 5. Spectral responses of synthesized transfer functions, using the coupling coefficients theoretically calculated, and with random $\pm 5\%$ variations.

A way to confirm how these variations affect the filter performance is making a random variation of all the coupling coefficients (K_s) with a uniform distribution between $\pm 5\%$ of the theoretically calculated values. In Fig. 5, are shown the eleven spectral results after doing this, ten with randomly generated K_s , and one with the ideal K_s . The ripple changes to 6 dB in the worst case and the crosstalk in less than 8 dB, see Fig. 5, maintaining a crosstalk at least of 46.5 dB, a very good merit figure.

These variations also represent changes of the spectral response magnitude of less than 7 dB in passband, see inset of Fig. 5, and 3.6 dB in the stopband if the worst case is considered.

5.2 Poles frequency dependence

The MIARR shows also a singular property, its poles module frequency dependence. As it can be seen in Eq. (17), this is due to the gratings reflectivity frequency dependence. This property means a better crosstalk for our device.

To know how the frequency dependence poles improve the crosstalk, we must first know the effect of fix poles (non frequency dependent poles) in the spectral response of a discrete time transfer function. It is known [22] the spectral periodicity of discrete time systems transfer functions. Being dominated the spectral response by the poles position in the Z plane; moreover when this is an all pole transfer function, as in our case. If the poles are near the unitary circumference the peaks are greater [22], being peaks amplitude inversely proportional to the poles distance to the unitary circumference. Appearing in frequencies given by Eq. (15), with φ_z changed by the poles phase φ_p , see Eq. (18). Now when we calculate the spectral response we change z by $e^{j\Omega\tau}$ and rotate the phasor $e^{j\Omega\tau}$ over the unitary circumference, calculating the transfer function value for each frequency. The position of the poles is the same in each rotation, which means peaks of the same amplitude and in the same frequency location by period. Then a periodic spectral response is generated.

On the other hand, when we have frequency dependent poles, their values change in frequency (changing in each rotation), being different in each period (FSR). For an ideal DG (box like spectrum), we would have poles with the desired value for FSRs inside of FWHM of

DG, and zero value poles for FSR outside it. These poles module change, varies the peaks amplitude in and out the FWHM, breaking the spectral periodicity.

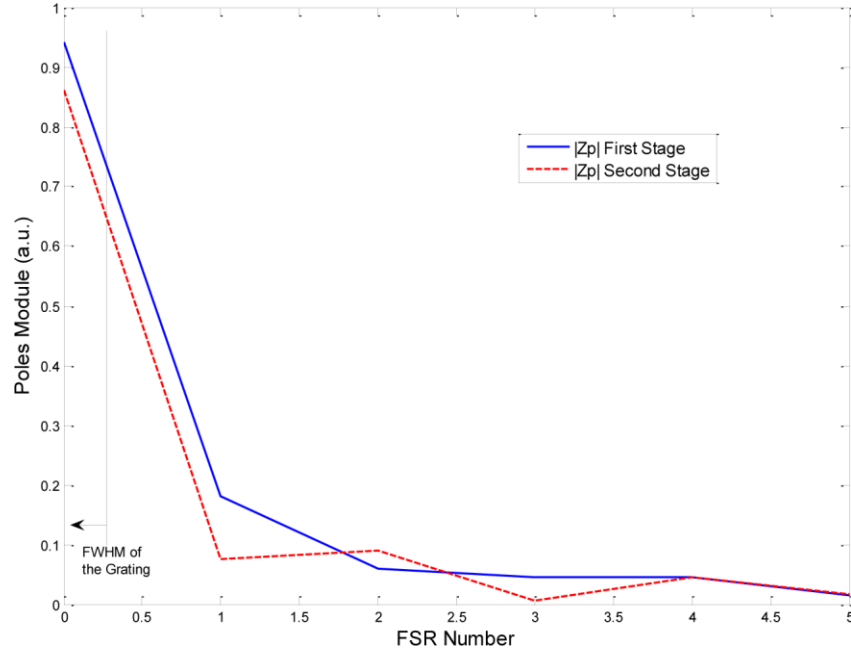


Fig. 6. Poles module value for two stages MIARR filter of previous section example, for each FSR. FSR 0 correspond to FSR including f_G .

In Fig. 6 is shown the poles module in each FSR, for the two stages MIARR example given in the previous section. In this figure, the x axis 0 value corresponds to the FSR including the f_G . As we can see the poles module diminishes once you move from the 0 FSR to greater (or smaller) FSR. This diminishing e.g. in the first stage pole module, from the FSR 0 to FSR 1, could represent a peak variation of 11 dB.

The spectral response of the synthesized filter will be equal to that of the desired filter inside DG FWHM. But out of it, the poles will move far inside from the unitary circumference, see Fig. 6. As a result, there are resonance peaks smaller than the resonance peaks inside the DG FWHM, increasing the crosstalk, in comparison e.g. with a cascaded DG and a fourth order delay line filter.

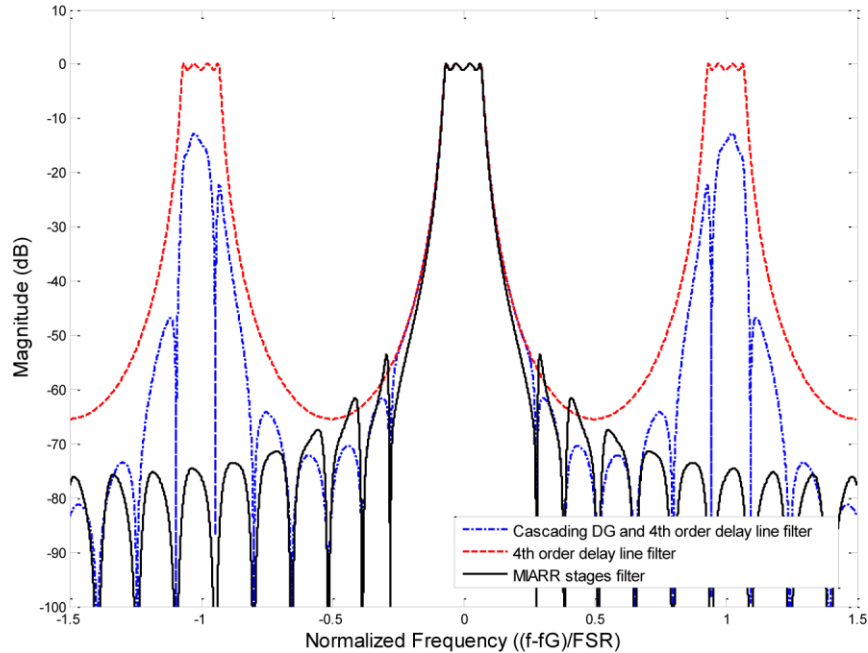


Fig. 7. Spectral responses of MIARR stages filter, fourth order periodic delay line filter, and cascading DG with fourth order filter.

In Fig. 7, it can be seen the spectral responses of the synthesized filters using the MIARR stages, and cascading a DG with a fourth order periodic delay line filter. As we see the cascading and MIARR stages spectral responses have the same performance in the 0 FSR, but in -1 and 1 FSRs, the cascade filter effect of DG only attenuates the signal 12.8 dB, while the MIARR stages filter attenuates the signals in more than 65 dB. This attenuation is mainly due to two mechanisms: the poles frequency dependence and the gratings transfer function module that appears in the numerator of Eq. (10). As we can see the less value of the poles module in the -1 and 1 FSRs, decreases the peaks of the spectral response, increasing the crosstalk, while the term in numerator of Eq. (10) acts like a cascaded DG, being responsible of an attenuation of 25.6 dB (two stages). The frequency dependent poles are responsible of more than 40 dB of attenuation.

6. Conclusion

A novel filter synthesis method is reported for designing flexible, tunable, ultra-large FSR filters. Filters with flat response, high crosstalk values and low ripple are reported. It can be used as part of optical cross-connects for selecting DWDM channels avoiding very restrictive FSR (inversely proportional to ring length). Closed equations for poles location and tuning are reported. Diffraction gratings structures are designed to suppress the resonances of the RR at both sides of the main wavelength. The use of gratings inside RR has allowed for significantly enhancing the suppression of resonances inside the simple RR FSR. Isolation values with non-extracted bands higher than 54 dB and a transmission ripple in the through port less than 1.3 dB are reported. This filter configuration can also be hitless reconfigured by shifting the position of the gratings and RR by changing their refractive index. A novel optical filter design method, based on all-poles transfer functions, and allowing the design of any type of optical digital filter is also reported. Robustness to coupling coefficient fabrication tolerances of the couplers from $\pm 5\%$ are validated in a specific design. Crosstalk improvement of 40dB because of pole frequency dependence in comparison with serial gratings configuration outside RR, is also reported.

Acknowledgments

Financial support by the European Commission under project BONE grant n°. ICT-216863 and Spanish MCyT under contract TEC2009-14718-C03-03 is acknowledged. Also we acknowledge the grant given by SENACYT, to one of the authors.